Journal of Luminescence 171 (2016) 254–258

Contents lists available at ScienceDirect

Journal of Luminescence

journal homepage: www.elsevier.com/locate/jlumin

Full Length Article

Afterglow properties of CaF_2:Tm nanoparticles and its potential application in photodynamic therapy

M. Zahedifar [a,b,*], E. Sadeghi [a,b], M.M. Shanei [b], A. Sazgarnia [c], M. Mehrabi [b]

[a] Physics Department, University of Kashan, Kashan, I.R. Iran
[b] Institute of Nanoscience and Nanotechniology, University of Kashan, Kashan, I.R. Iran
[c] Research Center and Department of Medical Physics, School of Medicine, Mashhad University of Medical Sciences, Vakil Abad Blvd., Mashhad, Iran

ARTICLE INFO

Article history:
Received 11 November 2014
Received in revised form
15 August 2015
Accepted 16 November 2015
Available online 3 December 2015

Keywords:
CaF_2:Tm
Nanoparticles
Afterglow
Photodynamic therapy

ABSTRACT

CaF_2:Tm nanoparticles (NPs) were synthesized by the hydrothermal method. Intense afterglow emission with long life time was found for the produced NPs, so its applicability in photodynamic therapy was investigated. Since the wavelength of the afterglow emission of the NPs fairly matches with the absorption band of the PpIX sensitizer, especially in the red region, the Cystein mediator was used to bond NPs with the PpIX sensitizer. The CaF_2:Tm NPs conjugated with PpIX was exposed to X-ray and by using the Antracene as detector, the production of the singlet oxygen was verified. Therefore, the produced NPs are recommended as a source of energy that improves photodynamic therapy beyond its current limitations.

1. Introduction

Cancer is a malignant type of disease characterized by cells that show uncontrolled growth and have the ability to invade and destroy other tissues. Different traditional treatments for cancer include surgical removal of tumor tissue [1], chemotherapy using compounds that are toxic principally to rapidly growing cells [2] and radiation therapy, where ionizing radiationis directed to the tumor and disrupts the replication of its genetic material [3]. In addition, surgery, chemotherapy and radiotherapy all tend to be immunosuppressive and limit due to risk of cosmetic and functional damage [4]. Photodynamic therapy (PDT) is an emerging alternative to radiation therapy and surgical resection [5]. PDT has been designated as a promising new strategy in the treatment of cancer since the early 1980s [6]. The main advantages of PDT over other techniques are the selectivity of drug accumulation in tumor, the ability to focus the light on the tumor region and the absence of toxicity caused by the drug alone [7]. PDT is a treatment modality that combines a photosensitizing agent with a proper wavelength of light in order to selectively destroy cells. The interaction of photons with photosensitizers in the presence of oxygen molecules, results in the formation of reactive oxygen species (ROS), such as singlet oxygen ($^1O_2$), or free radicals, which can then render apoptotic and necrotic cell death [7,8]. The generation process of ROS has been reviewed in detail [9].The efficiency of PDT is determined by the ROS production which depends on several parameters including the photosensitizer used, light intensity and wavelength and oxygen concentration [10].

During the past few decades, various types of photosensitizer molecules have been synthesized. Many organic dyes, porphyrins and derivatives, flavins and other biomolecules are efficient sensitizers [11]. Porphyrins, chlorines and bacteriochlorins are among the most useful photosensitizers [12]. In 1961 the capacity of Hematoporphyrin derivatives (HpD) to induce a cytotoxic effect in the presence of light with an appropriate wavelength was reported. HpD have been the only photosensitizers used in human clinical studies [13]. Protoporphyrin IX (PpIX) is an efficient hydrophobic sensitizer that is activated by light. The subsequent interaction of activated PpIX with molecular oxygen produces cytotoxic ROS, particularly singlet oxygen ($^1O_2$), that causes irreversible destruction of the target tissue [14–16].

Despite the advantage of PDT over some other techniques, there are two important limitations on PDT, the first one is the side effects of the photosensitizers, and the second is the lack of penetration of visible light in tissues. Therefore, it seems logic to look for new modalities in order to decrease undesired side effects, and at the same time to increase the depth of treatment [17]. To solve the problem of light penetration and enhance the PDT treatment for deep cancers, afterglow NPs has been used. The advent of nanosciences opened up new possibilities for PDT

* Corresponding author at: Physics Department, University of Kashan, Kashan, I.R. Iran. Tel.: +98 31 55912577; fax: +98 31 55912570.
E-mail address: zhdfr@kashanu.ac.ir (M. Zahedifar).

http://dx.doi.org/10.1016/j.jlumin.2015.11.043
0022-2313/

[18,19], where NPs were used as highly sophisticated, multifunctional medicines. Theoretically, NPs have potential to improve PDT beyond its current limitations [20].

Afterglow or long-lasting phosphors are doped materials, particularly rare earth-doped materials, with persistent light emission after cessation of excitation [21,22].The afterglow mechanism is related to electron traps, so afterglow luminescence remains from several seconds to hours or is required to overlaps with the absorption wavelength of the photosensitizer [23]. Recently, afterglow NPs such as CaF_2:Eu, ZnO, CdS, ZnS:Cu, Co and LaF_3:Tb were suggested as light source for PDT activation [24–26]. CaF_2:Tm NPs have unique luminescence characteristics which render to use for PDT. In this work, a new PDT mediated by CaF_2:Tm afterglow NPs is designed for the first time in which the light is generated by NPs with attached photosensitizers.

2. Materials and methods

The raw materials used for synthesis of CaF_2:Tm NPs were Ca $(NO_3)_2$ (of 99.95% purity), NH_4F (of 99.9% purity), $Tm(NO_3)_3$ (of 99.99% purity), Brij 35 (of 99.9% purity) and distilled deionized water, ethanol and methanol (all from Merck Chemicals). Protoporphyrin (PpIX) and L-Cystein were produced from Sigma-Aldrich, Germany and EDC (ethyl dimethylaminopropyl carbodiimide), NHS (N-Hydroxy succinimide), DMSO and Anthracen from Fluka, Switzerland. The hydrothermal method was used for preparation of CaF_2:TmNPs based on following reaction [27].

$$Ca(NO_3)_2 + 2NH_4F \rightarrow CaF_2 + 2NH_4(NO_3)$$

The solution of Brij 35 surfactant and calcium nitrate were prepared by mixing them slowly while was placed on a stirrer. Thulium nitrate and L-cysteine were added to the above solution and finally the ammonium fluoride was included very slowly while stirred. The final mixture was placed in an autoclave at 200 °C for 12 h, followed by cooling. The solid part was collected by centrifuging the product mixture and was washed with deionized water for several times. The obtained nanostructures were dried in an oven for 2 h at 150 °C. Then the solution of EDC was added to protoporphyrin (PpIX) in DMSO drop by drop while stirring and after 10 min, NHS was added slowly. Then the solution of CaF_2:Tm NPs conjugated to L-Cystein, were added to the last solution of PpIX and EDC dropwise. The stirring was continued for 24 h. Finally, the conjugates of CaF_2:Tm NPs with PpIX were separated by centrifuging and purified by washing with ethanol.

3. Characterization

The structural characterization of the synthesized sample was supported by X-ray diffraction (XRD) with RigakuD-maxcIII diffractometer using CuK_α radiations. SEM images were obtained using a scanning electron microscope model Philips XL-30 ESEM equipped with energy dispersive spectrometer (EDS). UV–visible absorption spectroscopic measurements were recorded by Shimadzu UV1700 spectrometer. In addition, infrared measurements were recorded on a Buck 100 instrument using KBr pellets at room temperature. Photoluminescence (PL) spectrum was recorded using a Perkin-Elmer spectrometer model LS55 with photo multiplier tube and Xenon lamp at room temperature. For afterglow measurements, a 20 W UV lamp from Nitride Semiconductors Co., with an irradiation peak at 250 nm and a100 kVp, 80 mA X-ray facilities with 1 Gy/min irradiation dose rate were used as excitation sources. Afterglow emission spectra and decay curves were detected using a cooled electro-optic spectrometer (Thermo-Electric cooled and regulated CCD, Avantec Co., NL-6961 RB Eerbeek, the Netherlands). The Ava Spect-2048 × 14 Fiber Optic Spectrometer was a back-thinned type CCD spectrometer with high quantum efficiency and high UV sensitivity.

4. Results and discussion

As stated in Section 2, the synthesis procedure and characterization of CaF_2:Tm NPs has been reported earlier by our team [27]. X-ray diffraction (XRD) pattern of CaF_2:Tm NPs is shown in Fig. 1. XRD analysis of the NPs showed a cubic lattice structure in correspondence with the ICSD collection code no. 060368 which is observed below the figure.

The broad peak in low angle region is due to the glass which was used as cell in XPD process.The crystalline size of CaF_2:Tm NPs was estimated using the Scherer's formula which was calculated to be approximately 40 nm. In order to further reveal the size and the shape of the prepared CaF_2:Tm NPs, the SEM images were utilized

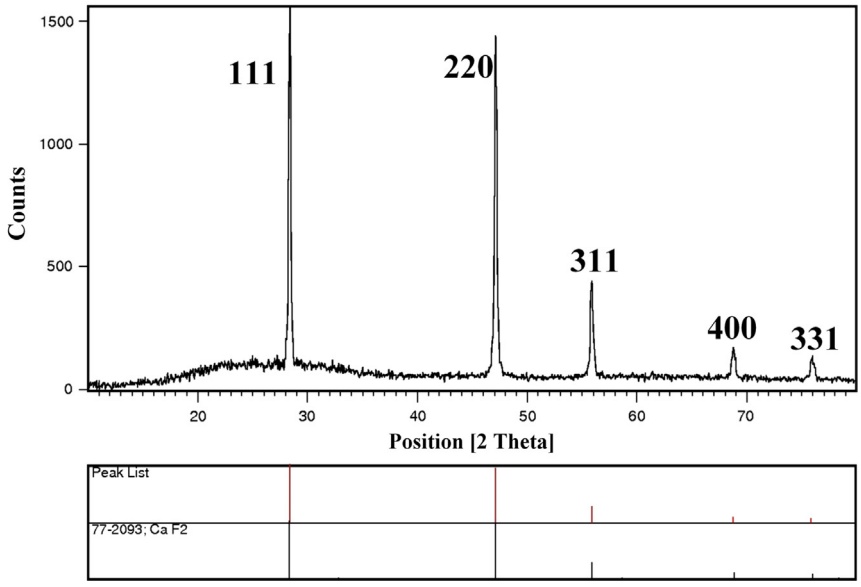

Fig. 1. X-ray diffraction (XRD) pattern of CaF_2:Tm NPs. The position of XRD peaks of the bulk CaF_2 crystalline are shown at the below.

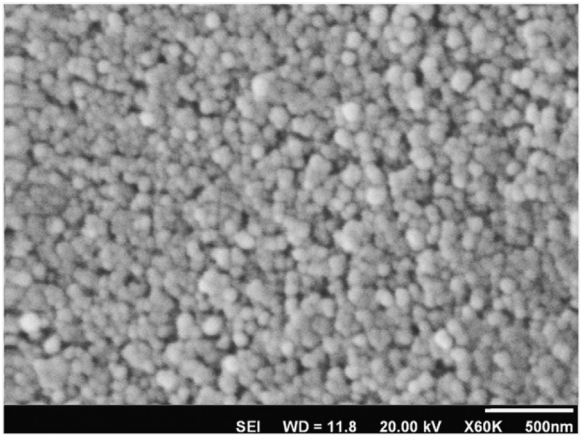

Fig. 2. SEM image of the produced CaF_2:Tm which shows a well dispersed NPs with an average size in accordance with that obtained from XRD analysis.

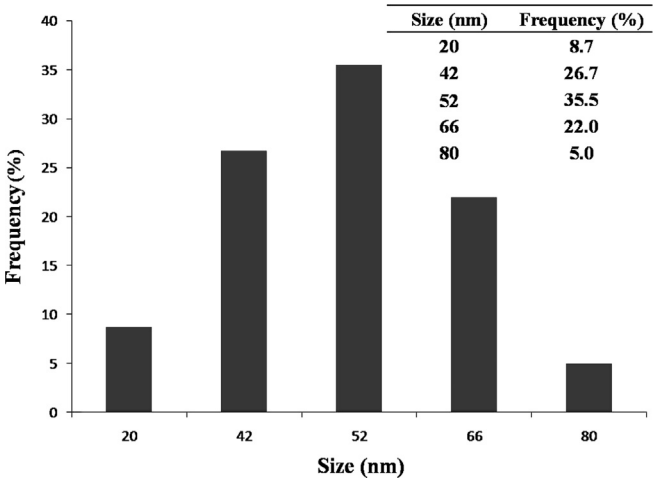

Fig. 3. The size histogram of the produced CaF_2:TmNPs.

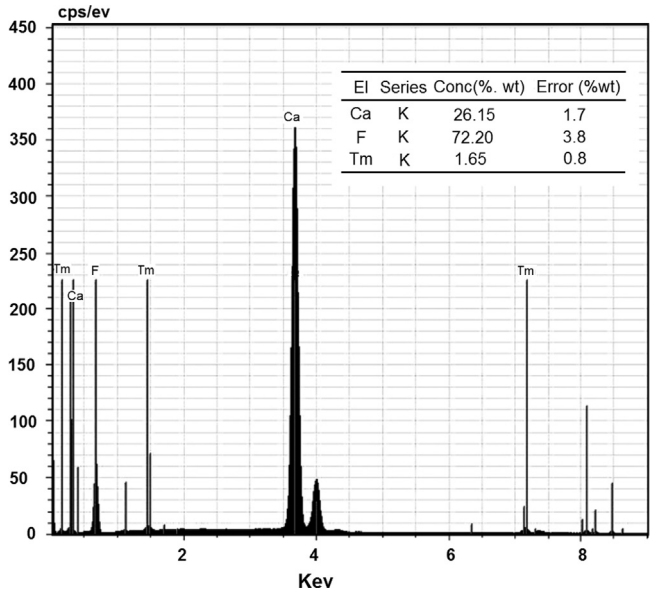

Fig. 4. EDS spectrum of CaF_2:Tm NPs. The elemental concentrations are seen as inset of the figure.

which is observed in Fig. 2. As is obvious, the scatter in the particle size is not considerable. This is justified by the size histogram in Fig. 3 and the average size is in agreement with the calculated one.

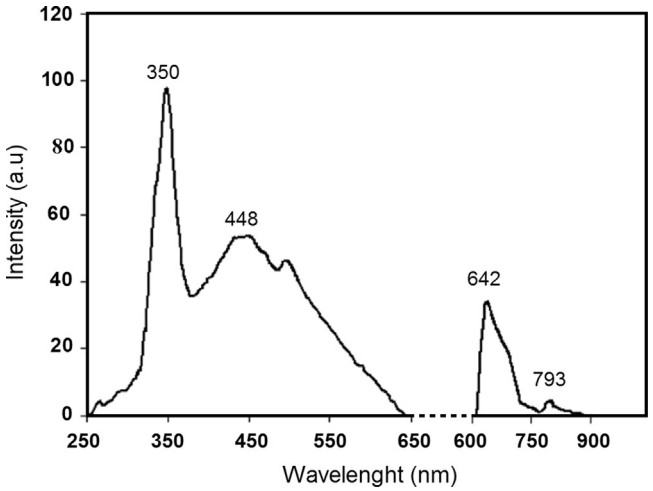

Fig. 5. The emission spectra of CaF_2:Tm NPs. Four strong emission bands at 350, 448, 642 and 793 nm are present in the PL emission of the synthesized NPs.

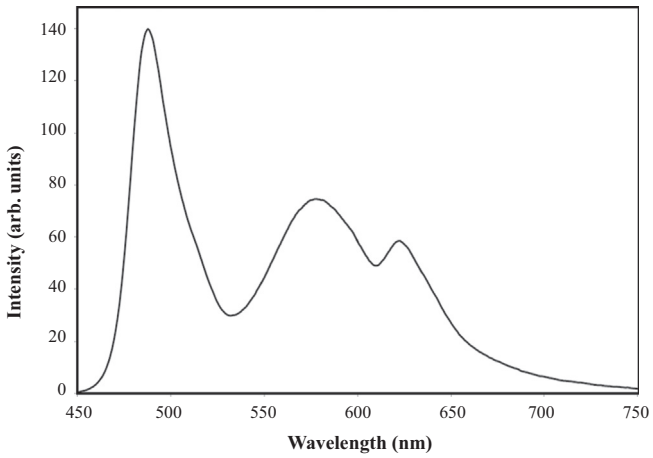

Fig. 6. Afterglow of CaF_2:Tm NPs. The spectrum was recorded following UV irradiation at 250 nm for 1.5 min.

EDS spectrum of CaF_2:Tm NPs is seen in Fig. 4 and the elemental concentrations are seen as inset of the figure. Optical properties and energy transfer of thulium doped nanocrystals [28–30] and thulium doped calcium fluoride nanostructure [31–33,27] have been reported. Fig. 5 shows the emission spectra of CaF_2:Tm NPs. Four strong emission bands at 350, 448, 642 and 793 nm are there in the PL emission of the synthesized NPs. Similar emission bands can be observed in previously reported emission spectra of Tm doped nanoparticles [28,29,31]. The CaF_2:Tm NPs were excited by UV lamp for 1.5 min and the measurement of afterglow was performed at room temperature. Introduction of Tm ions into CaF_2 host produces a highly dense trapping level at appropriate depth, which may be considered to be responsible for the long-lasting phosphorescence at room temperature.

The afterglow spectrum is shown in Fig. 6. Three emission peaks at 488, 582 and 628 nm are seen in this figure. The decay life time is defined as the time when the afterglow reaches its half-intensity and the longevity as the time when the afterglow is totally disappears [34]. Fig. 7 shows the afterglow decay curves at 488, 582 and 628 nm. The decay life time and longevity at 628 nm are more than those of 582 nm and 488 nm emission bands.

X-ray is a well-known electromagnetic radiation which is capable to penetrate human tissues and has already been widely used in many applications including cancer treatment [35]. While UV light is a good excitation source, CaF_2:Tm can also be excited by

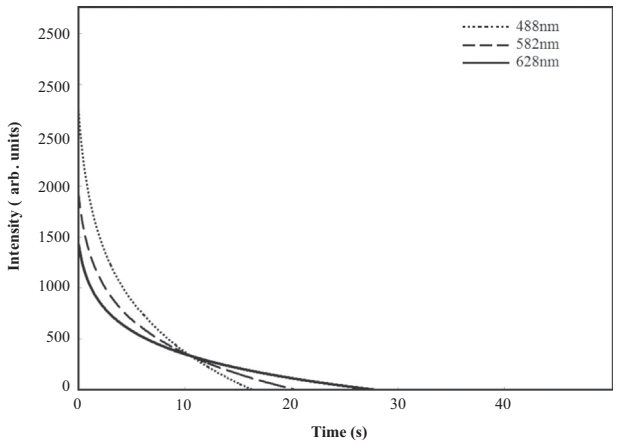

Fig. 7. Afterglow decay curves of CaF_2:Tm NPs monitored at 488, 582 and 628 nm. The spectra were taken after UV irradiation at 250 nm for 1.5 min.

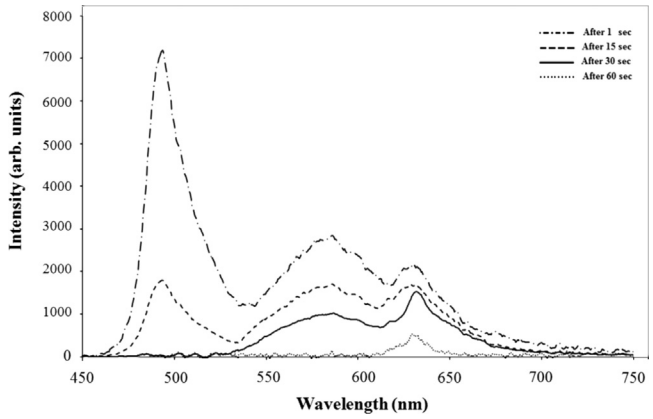

Fig. 8. Afterglow spectra of CaF_2:Tm NPs for different time intervals of 1, 15, 30 and 60 sec between excitation and recording the spectra. NPs were excited by the X-ray for 1.5 min with dose rate of 0.5 Gy/min.

X-ray to improve its afterglow intensity and persistent time by possibly creating some defects and it seems to be more possible to explain this emission via different defects formation by X-ray irradiation.

Fig. 8 shows the afterglow emission spectra of CaF_2:Tm NPs at 1, 15, 30 and 60 s after the X-ray excitation was turned off. The spectra were recorded by the exposure of X-ray for 1.5 min with an approximate dose rate of 1 Gy/min. The afterglow spectra measured by UV and X-ray excitation have similar emission bands but different intensity due to the fact that with increasing the energy of excitation source, the amount of electron–hole pairs are increased, resulting in a longer decay life time.

Fig. 9 demonstrates the afterglow decay curve of the CaF_2:Tm NPs (excited by X-ray) at 488, 582 and 628 nm which has longer life time than those of Fig. 7. As discussed above, the increase in the life time is due to the energy of the X-ray excitation source.

Afterglow of water-soluble NPs opens up new applications in photodynamic therapy. The afterglow of CaF_2:Tm NPs generates proper light which can active photosensitizer for PDT. PpIX photosensitizers with two strong absorption bands around 400 and 630 nm have been used in human clinical studies [17,18]. Afterglow spectrum of synthesized NPs perfectly matches the absorption spectrum of PpIX at around 630 nm, so the transferred energy from the NPs can activate the photosensitizer. In this work, PpIX-Cystein-CaF_2:Tm NPs were designed, synthesized and characterized, in order to apply it for in vitro tests in PDT of cancer cells. PpIX-conjugated CaF_2:Tm NPs were prepared using L-Cystein as

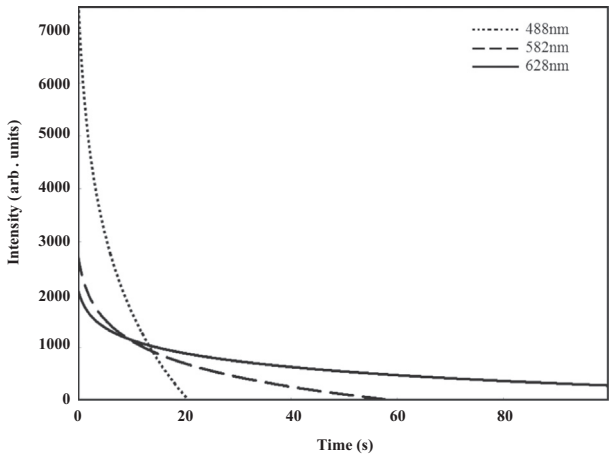

Fig. 9. Afterglow decay curves of CaF_2:Tm NPs, monitored at 488,582 and 628 nm after an administrated dose of 1.5 Gy by X-ray.

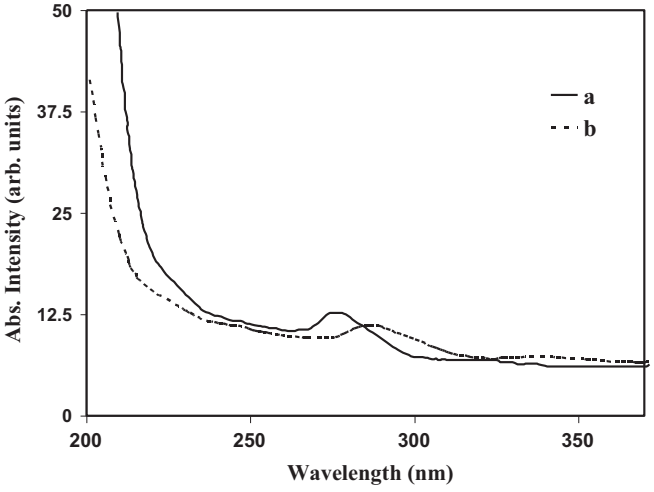

Fig. 10. UV–Visible absorption spectra of CaF_2:Tm NPs (a) and PpIX-Cystein-CaF_2:Tm NPs (b). A red shift is seen in the absorption peak of PpIX-Cystein-CaF_2:Tm NPs at 275 nm relative to CaF_2:Tm NPs.

the linker. Molecules with bifunctional groups, such as L-cysteine, which are known as functional ligands are used to link the NPs tophotosensitizers. Cystein reacts with PpIX in the presence of EDC at room temperature to form PpIX-conjugated L-Cystein. Fig. 10 (a, b) show the UV–visible spectra of the synthesized CaF_2:Tm NPs and PpIX-Cystein-CaF_2:Tm NPs respectively. A red shift is seen in the absorption peak of PpIX-Cystein-CaF_2:Tm NPs at 275 nm relative to CaF_2:Tm NPs. There is not direct experimental evidence on the cause of this red shift. However, considering this red shift as a result of conjugating PpIX-Cystein to the CaF_2:Tm NPS, it is likely that the complex PpIX-Cystein-CaF_2:Tm with a larger size than CaF_2:Tm NPS is responsible for this absorption band.The conjugation of PpIX-Cystein-CaF_2:TmNPs was proved by IR spectroscopy.

An important features of the singlet oxygen is the emission band at 1250 nm, however because of its very short life time (from order of microsecond), complicated methods are required to detect it straight. Therefore, an indirect method was used to detect the singlet oxygen. Antracene has an emission band following excitation at 360 nm and reacts with the singlet oxygen in the medium to give antrakinon. Taking into consideration that the antrakinon has not any emission band, the Antracene can be used for detecting the singlet oxygen. For guarantee the capability of the synthesized NPs to produce singlet oxygen, PpIX conjugated

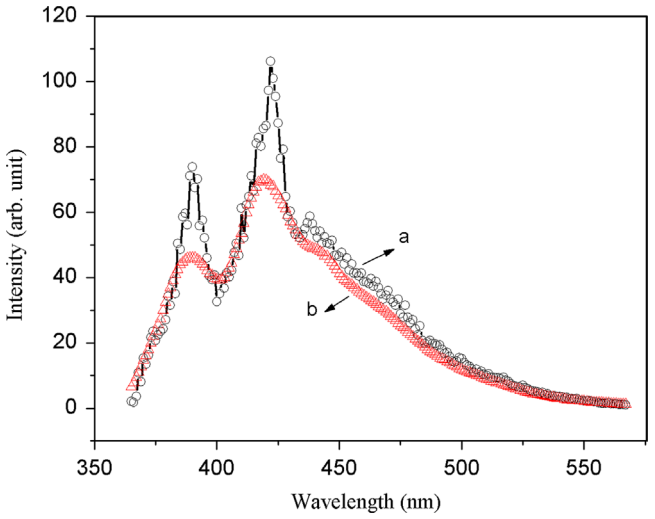

Fig. 11. PL emission of the Antracene after irradiating the sample to 1.5 Gy X-ray dose and exciting with the wavelength of 360 nm (a) and solution of Antracene and CaF_2:Tm nanoparticle conjugated to PpIX and irradiated to the same X-ray dose of 1.5 Gy followed by excitation with the wavelength of 360 nm (b). A considerable decrease in PL intensity of Fig. 11(b) is observed.

CaF_2:Tm NPs were exposed to X-ray and then the activation of PpIX and production of the singlet oxygen were studied with measuring the decrease in the fluorescence intensity of the Antracene ($C_{14}H_{10}$). Fig. 11(a) shows the PL spectrum of the Antracene after an administrated dose of 1.5 Gy from X-ray source. For recording the PL pattern, the sample was excited to the wavelength 360 nm.This figure was used as reference for verifying the capability of the NPs to produce singlet oxygen.

The phosphorescence spectrum of CaF_2:Tm NPs contains three emission peaks at 488, 582 and 628 nm. From the above emission bands, only the longer wavelength at 628 nm matches with the absorption band of the PpIX. This emission band as is evident in Fig. 9, has longer life time compared to other emission bands and can activate PpIX. To examine this potential, the solution of Antracene, PpIX and CaF_2:Tm NPs was exposed to X-ray for 3 min with a dose rate of 0.5 Gy/min. Then the emission spectrum of the Antracene was obtained following excitation at 360 nm. The result is shown as Fig.11(b). As is evident in this figure, the emission band of the Antracene demonstrates a considerable decrease compared to Fig. 11(a), an indication of production of the singlet oxygen by the CaF_2:TmNPs conjugated with the PpIX sensitizer.

5. Conclusion

Considering the long life time of afterglow emission of CaF_2:Tm NPs (at 488, 582 and 628 nm), especially for the wavelength at 628 nm and that this emission band fairly matches with the absorption peak of the PpIX sensitizer, this nanopaticle was conjugated to PpIX sensitizer to examine the capability of the complex of PpIX-CaF_2:Tm NPs to produce the singlet oxygen. By irradiating the product with X-ray photons, the singlet oxygen was detected indirectly. The production of the singlet oxygen was verified by a complementary experiment using the Antracene as detector.Therefore, the afterglow CaF_2:Tm NPs are recommended to solve the problem of light penetration and enhance the PDT treatment for deep cancers.

Acknowledgment

Authors are grateful to research council of the University of Kashan for providing financial support to undertake this work.

References

[1] Z. Dobronte, T. Wittmann, G. Karácsony, Endoscopy 10 (1978) 127.
[2] M. Dean, T. Fojo, S. Bates, Nat. Rev. Cancer 5 (2005) 275.
[3] L.H. Gray, A.D. Conger, M. Ebert, S. Hornsey, O.C. Scott, Br. J. Radiol. 26 (1953) 638.
[4] A. Master, M. Livingston, A. Sen Gupta, J. Control. Release 168 (2013) 88.
[5] X. Liu, B.J. Chen, E.Y.B. Pun, H. Lin, J. Lumin. 137 (2013) 77.
[6] I.J. Macdonald, T.J. Dougherty, J. Porphyrins Phthalocyanines 5 (2001) 105.
[7] R. Allison, T.S. Mang, B.D. Wilson, Semin. Cutan. Med. Surg. 17 (1998) 153.
[8] S. Wang, R. Gao, F. Zhou, M. Selke, J. Mater. Chem. 14 (2004) 487.
[9] F. Wilkinson, W.P. Helman, A.B. Ross, J. Phys. Chem. Ref. Data 22 (1993) 113.
[10] L. Yang, Y. Wei, D. Xing, Q. Chen, Lasers Surg. Med. 42 (2010) 671.
[11] R.W. Redmond, J.N. Gamlin, Photochem. Photobiol. 70 (1999) 391.
[12] B.D. Wilson, T.S. Mang, M. Cooper, H. Stoll, Facial Plast. Surg. 6 (1988) 185.
[13] R.L. Lipson, E.J. Baldes, A.M. Olsen, J. Natl. Cancer Inst. 26 (1961) 1.
[14] N. Suzuki, S. Okada, S. Chida, C. Komori, Y. Shimada, T. Suzuki, Anticancer Res. 27 (2007) 4179.
[15] Q. Liu, X. Wang, P. Wang, L. Xiao, Q. Hao, Cancer Chemother. Pharmacol. 60 (2007) 671.
[16] E.R. Reis, K. Metze, E.M.D. Nicola, I.E. Borissevitch., J. Lumin. 137 (2013) 32.
[17] Z. Luksiene, Medicina 39 (2002) 1137.
[18] C. Liu, Nano Biomed. Eng. 1 (2009) 1.
[19] Y. Zhang, Nano Biomed. Eng. 3 (2011) 1.
[20] T. Nann, Nano Biomed. Eng. 3 (2011) 137.
[21] T. Aitasalo, P. Deren, J. Holsa, H. Jungner, J. Krupa, M. Lastusaari, J. Legendziewicz, J. Niittykoski, W. Strek, J. Solid State Chem. 171 (2003) 114.
[22] E. Nakazawa, S. Shionoya, W.M. Yen, Handbook of Phosphor, CRC Press, Washington DC, 1999.
[23] P. Juzenas, W. Chen, Y.P. Sun, M.A.N. Coelho, R. Generalov, N. Generalova, I. L. Christensen, Adv. Drug. Deliv. Rev. 60 (2008) 1600.
[24] W. Chen, J. Biomed. Nanotechnol. 4 (2008) 369.
[25] W. Chen, J. Zhang, J. Nanosci. Nanotechnol. 6 (2006) 1159.
[26] Y. Liu, W. Chen, S. Wang, A.G. Joly, Appl. Phys. Lett. 92 (2008) 043901.
[27] M. Zahedifar, E. Sadeghi, Radiat. Phys. Chem. 81 (2012) 1856.
[28] M. Quintanilla, N.O. Núñez, E. Cantelar, M. Ocaña, F. Cussó, Nanoscale 3 (2011) 3.
[29] F. Abdulá Rahim, RSC Adv. 3 (2013) 21.
[30] Z. Xiang-Yu, Z. Hai-Rong, G. Dang-Li., Chin. Phys. 17 (2008) 11.
[31] N. Salah, N.D. Alharbi, S.S. Habib, S.P. Lochab, J. Nanomater. 2015 (2015) (Article ID 136402).
[32] W. Chen, J. Zhang, U.S. Patent Application 11/347,075.
[33] Y. Kishi, S. Tanabe, S. Tochino, G. Pezzotti, J. Am. Ceram. Soc. 88 (2005) 12.
[34] L. Ma, W. Chen, Nanotechnology 21 (2010) 385604.
[35] R. Lewis, Phys. Med. Biol. 42 (1997) 1213.